galaxies

MDPI

Review

Mass Loss in Be Stars: News from Two Fronts

Alex C. Carciofi [1,*], Guilherme P. P. Bolzan [1], Pâmela R. Querido [1], Amanda C. Rubio [1,2], Jonathan Labadie-Bartz [3,4], Tajan H. de Amorim [1], Ariane C. Fonseca Silva [1] and Vittória L. Schiavolim [1]

[1] Instituto de Astronomia, Geofísica e Ciências Atmosféricas, Universidade de São Paulo (IAG/USP), Rua do Matão 1226, Cidade Universitária, São Paulo B-05508-900, SP, Brazil; guilhermeppbolzan@usp.br (G.P.P.B.); querido@usp.br (P.R.Q.); amanda.rubio@usp.br (A.C.R.); tajan.amorim@usp.br (T.H.d.A.); arianecristina@usp.br (A.C.F.S.); vittoriaschiavolim@usp.br (V.L.S.)
[2] Max-Planck-Institut für Astrophysik, Karl-Schwarzschild-Str. 1, 85748 Garching bei München, Germany
[3] LIRA, Observatoire de Paris, Université PSL, CNRS, Sorbonne Université, Université Paris Cité, CY Cergy Paris Université, 92190 Meudon, France; jbartz@udel.edu
[4] DTU Space, Technical University of Denmark, Elektrovej 327, DK-2800 Lyngby, Denmark
* Correspondence: carciofi@usp.br

Abstract

Be stars are characterized by the presence of a circumstellar Keplerian disk formed from material ejected from the rapidly rotating stellar surface. This article presents recent observational and theoretical progress on two central aspects of this phenomenon: the mechanisms driving mass loss, and the fate of the ejected material. Using simultaneous TESS photometry and ground-based spectroscopy, we examine the short-term variability associated with discrete mass ejection events, or "flickers", and review strong evidence linking them to pulsational activity near the stellar surface. Complementary 3D hydrodynamic simulations reproduce key observational signatures and establish that disk formation requires compact and asymmetric ejection sites with sufficient angular momentum to overcome re-accretion. In systems with binary companions, new high-resolution simulations resolve the outer disk for the first time and identify five dynamically distinct regions, including a circumsecondary disk and a circumbinary spiral outflow. Together, these results provide a coherent framework that traces the full life cycle of disk material from pulsation-driven ejection near the stellar surface to its final destination, whether re-accreted by the companion or lost from the system entirely.

Keywords: Be stars; mass loss; emission-line; winds; outflows; spectroscopic; photometry; circumstellar matter; disks

check for updates

Academic Editor: Sun Kwok

Received: 21 May 2025
Revised: 28 June 2025
Accepted: 3 July 2025
Published: 7 July 2025

Citation: Carciofi, A.C.; Bolzan, G.P.P.; Querido, P.R.; Rubio, A.C.; Labadie-Bartz, J.; de Amorim, T.H.; Fonseca Silva, A.C.; Schiavolim, V.L. Mass Loss in Be Stars: News from Two Fronts. *Galaxies* **2025**, *13*, 77. https://doi.org/10.3390/galaxies13040077

Copyright: © 2025 by the authors. Licensee MDPI, Basel, Switzerland. This article is an open access article distributed under the terms and conditions of the Creative Commons Attribution (CC BY) license (https://creativecommons.org/licenses/by/4.0/).

1. Introduction

Mass loss in stars is quite literally a universal phenomenon. Ubiquitous across all kinds of stellar types and spectral classes, it derives from multiple mechanisms, some better understood than others. The most notable case is probably mass loss through stellar winds, which is known to accompany the evolution of intermediate- and high-mass stars throughout their lifetimes. Already starting on the pre-main sequence objects (e.g., Herbig Ae/Be [1]), winds continue to be relevant during the main sequence (MS) as well as post-main sequence phases such as blue supergiant, red supergiant, and Wolf–Rayet stages. In hot massive stars (O and early B-type) as well as intermediate-mass stars [2], this kind of mass loss is primarily caused by radiation pressure on metal lines—a process described by the line-driven wind theory developed by [3] and subsequently refined by many authors (e.g., [4–6]). As they evolve off of the MS, additional mass loss mechanisms come into

play. Red supergiants exhibit slow and dense winds, likely driven by a combination of pulsations and dust formation (e.g., [7]), while luminous blue variables (LBVs) can undergo eruptive episodes of intense mass loss (e.g., [8]). At later stages, Wolf–Rayet stars lose mass at extremely high rates via strong and optically thick winds (e.g., [9]), which are essential in stripping the star of its outer layers and shaping the final pre-supernova structure.

However, mass loss takes on a new dimension in Be stars, a subclass that includes both intermediate- and high-mass objects. Decades of observational evidence and modeling have revealed particular mechanisms that differ from those in other stars (at least in their combination), emphasizing that understanding this phenomenon is essential to interpreting their observables. As such, one of the main objectives in this subfield is to uncover how exactly these stars lose mass (discussed in Sections 1.2 and 2) as well as the ultimate fate of the ejected material (discussed in Section 3).

1.1. Defining the Object: Be Stars

A large fraction of B-type stars are, in fact, Be stars, that is, stars that show (or have shown in the past) Balmer emission lines in their spectra. These emission lines originate in a Keplerian decretion disk composed of material ejected from the star itself [10].

According to the leading hypothesis, this ejection can be explained as a combination of fast rotation speeds and non-radial pulsations, two essential characteristics that are present across the entire Be population. While Be stars are known to rotate rapidly, with the fastest rotation among non-degenerate stars [10], current evidence suggests that they are all subcritical rotators and exhibit a wide range of rotation rates [11]. Regarding pulsation, recent studies based on space photometry of large samples of Be stars clearly show that this phenomenon is ubiquitous [12]. The specific ways in which both of those factors influence mass loss will be discussed in Section 1.2.

The presence of such high rotation speeds raises the question of how Be stars acquire them in the first place. Historically, three main formation scenarios have been proposed: (i) Be stars are born as fast rotators [13]; (ii) they gain their high rotation rates through interaction with a companion [14]; and (iii) they evolve into fast rotators during the MS evolution [15].

In scenario (i), the Be star inherits its angular momentum from its natal molecular cloud, forming with significantly higher rotation speeds than other non-Be massive stars. For scenario (ii), formative Be stars are thought to begin as ordinary B-type companions to more massive stars, which is a common occurrence for intermediate- and high-mass stars [16]. As the primary evolves off the MS, it expands to fill the secondary's Roche lobe, initiating a phase of mass and angular momentum transfer [17]. During this interaction, the secondary star destined to become the Be star spins up due to the accreted angular momentum, while the donor star becomes increasingly stripped. The outcome for the donor depends on its initial mass, potentially resulting in a compact object or He-rich hot subdwarf (sdOB) star [14]. Such a scenario is also invoked to explain how Wolf–Rayet stars lose their outer shells, as opposed to the wind scenario explained in Section 1. This binary interaction scenario is supported by observational studies. For instance, [18] found a notable lack of Be stars with MS companions, while such companions are common for normal B-type stars. This result is expected if a significant number of Be stars are post-mass transfer systems, as its companion would no longer be a regular MS star. Another possible pathway involving stellar interactions involves close companions in hierarchical triple systems. In this context, dynamical interactions with the third body can induce inward migration of the inner binary, eventually leading to mass transfer, or in some cases a merger [19] These processes can spin up the primary star to near-critical rotation, providing the necessary conditions for the Be phenomenon. Recent population synthesis models

(e.g., [20]) suggest that such triple-induced pathways may account for a substantial fraction of systems that form stripped companions, consistent with the observed lack of Be binaries at separations where direct mass transfer is not expected.

Scenario (iii) also posits that Be stars begin their life as ordinary B-types, but states that structural changes occur as they evolve along the MS, most notably, growth of the inert helium core. This leads to a redistribution of mass within the star, changing its moment of inertia. To conserve angular momentum, the outer layers respond by spinning up, potentially reaching near-critical rotation rates without the need for external interaction [15,21]. Evolutionary models that include internal angular momentum transport via meridional circulation and shear instabilities support this mechanism, although its efficiency in producing the observed Be population is up for debate (see [22,23]). Of the three scenarios, this is the only one that is necessarily always present. Even if it may not account for the bulk of the rotation, it can prolong the life of a Be star as a fast rotator [24] by counterbalancing the angular momentum lost through the disk [25].

The relative importance of each formation scenario remains an open question. It may even depend on environmental factors tied to the properties of the parent molecular cloud that gave rise to the particular stellar cluster being analyzed. Studies have shown that characteristics of the star-forming environment such as turbulence, density, and metallicity can significantly influence the initial angular momentum distribution of stars, potentially affecting the likelihood of Be star formation [26]. Regardless of the origin of this rapid rotation, its presence has profound effects on the chemical composition and evolution of Be stars, distinguishing them from other B-type stars. Rapid rotation can lead to enhanced mixing processes within the stellar interior, altering surface abundances and extending the MS lifetime compared to non-rotating counterparts [24].

1.2. Mass Loss in Be Stars

All B-type stars exhibit mass loss through stellar winds during their MS lifetimes [6], and Be stars are no exception. Given this, several mechanisms based on radiative mass loss have been proposed over the years to explain the formation of Be disks. One prominent early model was the wind-compressed disk (WCD) scenario [27], in which radiatively driven winds from a rapidly rotating star are deflected toward the equatorial plane due to the conservation of angular momentum, leading to the accumulation of material in a disk-like structure.

However, subsequent observational and theoretical work has shown that radiative pressure alone is insufficient to produce the dense and long-lived Keplerian disks observed around Be stars. In particular, the WCD model predicts equatorial infall and fails to account for the angular momentum required to sustain a Keplerian disk. Combined with inconsistencies with spectroscopic and interferometric data, these limitations have led to the rejection of purely radiative mechanisms as the primary drivers of disk formation (e.g., [28,29]).

Despite not being able to explain the formation of Be disks, stellar winds do have significant effects on the disks themselves, making their expression quite unique for Be stars. As shown by [30] using ultraviolet observations, these stellar winds exhibit orientation-dependent behavior, appearing much stronger in shell stars (Be stars observed edge-on). Recent studies by [31,32] have further elucidated the impact of stellar winds on Be disks. Their simulations demonstrated that line-driven ablation can effectively erode the disk, particularly in early-type Be stars. This ablation process is so efficient in O-type stars that it likely accounts for the scarcity of observed Oe stars (O-type stars that present the Be phenomenon), as their disks are rapidly destroyed by the intense stellar radiation. Ablation (or lack thereof) is also commonly invoked as one of the mechanisms explaining

the increased Be fraction in metal-poor environments, where the absence of metals inhibits the formation of stellar winds, facilitating the formation of disks [33]. While disk ablation is recognized as a significant factor in disk dissipation, its exact role in the broader context of the Be phenomenon remains poorly understood.

Having discarded radiative means as a viable explanation, multiple studies have since proposed several mechanical mass loss mechanisms. Among these, models involving magnetically induced mass ejection [34] and convectively driven waves [35] have been proposed, but either lack sufficient observational support or fail to reproduce key characteristics of Be disks [36].

The scenario that has best withstood scrutiny is the combined action of Be stars' characteristic fast rotation speeds and non-radial pulsations [12,37,38]. Due to their fast rotation, Be stars maintain surface material—especially near the equator—with energies nearly sufficient to overcome the stellar gravitational well. The non-radial pulsations, on the other hand, are thought to provide the additional momentum or "trigger" needed to lift material off the stellar surface and inject it into orbit, particularly modes that couple effectively with the surface layers. While neither pulsations nor fast rotation appear to be sufficient alone, their interplay offers a compelling framework to explain the episodic and variable nature of mass ejection events that feed the circumstellar disk in Be stars (see, e.g., [10,28]).

One of the first studies to suggest a connection between mass loss and stellar pulsations was [37]. The first clear observational evidence came from [39], who studied the Be star μ Cen. Their work revealed that outbursts of mass ejection were closely linked to changes in the star's non-radial pulsation modes, with enhanced pulsational activity preceding or accompanying the disk feeding events. Further links are now abundant (see, e.g., [40]). Today, it is understood that mass loss events in Be stars tend to coincide with an increase in overall pulsational amplitude and complexity [12], reinforcing the idea that pulsations act as the crucial "final push" to launch material into the disk. In Section 2, we review recent results from both observations and models that shed further light on the elusive mass loss process in Be stars.

As the star injects mass and angular momentum into the disk, the structure expands further. After multiple proposed theories [36], it is now understood that the disk's internal dynamics are best described by the viscous decretion disk (VDD) model [41,42]. Most of the material injected at the base of the disk acts as an angular momentum donor through viscous shear interactions and ultimately falls back onto the star—up to 99.9% in some cases [43]. The remaining fraction, having acquired sufficient angular momentum, reaches larger orbits, contributing to the disk's overall radial growth.

Hydrodynamic models such as the VDD, supported by observations, demonstrate that both the build-up and dissipation of the disk proceed from the inside out [25,42,44–46]. In stars that are initially diskless, the inner regions fill rapidly following the onset of a mass outburst, while further expansion occurs at a much slower rate [42]. This behavior is highly variable; while some stars can sustain long-lived outbursts that maintain stable disks for years (e.g., β CMi, [47]), others exhibit short intermittent mass loss episodes (e.g., μ Cen [40]), and many fall somewhere in between. Consequently, dissipating disks can be "revived" by subsequent outbursts. See [48] for a recent study of a large sample of Be stars in the Magellanic Clouds.

A lingering question concerns the ultimate fate of the ejected material: the VDD model predicts that after mass loss is interrupted, the now-unsupported disk begins to dissipate, eventually vanishing completely. In Section 3, we review recent results suggesting that a fraction of this material may escape to the interstellar medium (ISM), while some may be accreted by a stripped binary companion. This would be a remarkable reversal, in which

matter originally lost by the donor star—formation scenario (ii) above—is later re-accreted by its own remnant via the disk of the Be star.

2. Mass Loss Front

Mass loss (in any star) often has direct observational counterparts. Historically, the most important source of information for mass loss in Be stars has been spectroscopy, with polarimetry and photometry—especially space-based—gaining more ground as of late. This section mainly discusses differential photometry and spectroscopy, as they relate more closely to recent developments. We also present unpublished data on the Be star 12 Vul that traces mass ejection in polarimetry.

With the advent of the Transiting Exoplanet Survey Satellite (TESS) mission [49], high-precision differential photometry has become available for hundreds of Be stars. This unprecedented dataset was analyzed in detail by [12], who studied the light curves for 430 Be stars located in the southern ecliptic hemisphere. In addition to their findings on pulsational properties and variability, the study reported the presence of flickers in 18% of the full sample, or 31% of early-type stars. Observationally, a flicker is defined as a deviation from the baseline photometric level that lasts from a few days to several weeks. In TESS data—collected through a broad-band filter covering the red part of the visible spectrum extending into the near-infrared—typical flicker amplitudes range from 0.1 to 0.3 magnitudes, although smaller and larger amplitudes are also seen. The vast majority of flickers are characterized by a net brightening, but a small number of dimming flickers having much lower amplitudes have also been observed. Furthermore, the growth phase is typically faster than the decay phase (see [12] for further details). These flickers are interpreted as the photometric counterpart of short-lived mass loss events, providing a unique window into the dynamics of disk feeding in real time. Despite their significance, photometric flickers are primarily sensitive to the amount of mass ejected, offering limited insight into the geometry and kinematics of the outflowing material.

To address this limitation, an ongoing campaign was launched in 2020 using the Network of Robotic Echelle Spectrographs (NRES [50]). This effort targets the most active stars identified in the TESS sample, aiming to complement the photometric data with spectroscopic diagnostics that can trace the structure and evolution of the ejected material in greater detail. The four-year effort succeeded in capturing around fifty flickers in thirteen Be stars observed simultaneously with both TESS and NRES, in addition to seven other events already reported in the literature, although these were only detected spectroscopically. One of the best-captured is for f Car, shown in Figure 1. According to the TESS data in the second row, this Be star displayed two photometric flickers: one of small amplitude, followed by another of larger amplitude. They are among the clearest flickers in the sample. Other cases exhibit multiple overlapping events, lack well-defined baselines and appear permanently active, or even maintain stable disks throughout the observed period, highlighting the wide diversity of photometric manifestations of mass loss in Be stars.

Both of f Car's flickers are also visible in the Hα equivalent width (EW, middle row). However, it is clear that the photometry varies more rapidly than the EW, suggesting that the former originates in a smaller volume closer to the stellar surface [51]. The fourth panel shows the line asymmetry calculated using the following formula:

$$\frac{\mathrm{EW_V}}{\mathrm{EW_R}} = \frac{\int_{-\infty}^{v_0} 1 - \frac{F_v}{F_C} dv}{\int_{v_0}^{\infty} 1 - \frac{F_v}{F_C} dv} \quad (1)$$

where v_0 is the systemic velocity of the star, F_v is the observed flux, and F_C is the continuum level; in addition, $\mathrm{EW_V}/\mathrm{EW_R}$ measures the net asymmetry of the line with respect to the line center. This metric has a distinct advantage over the traditional V/R[1] ratio commonly used

in Be star research, as it can be applied to any type of line profile. Indeed, even moderate departures from a clean double-peaked Hα profile render the V/R ratio unreliable [52]. A striking behavior seen not only in f Car but in all stars of the sample is that the line becomes strongly asymmetric during the rising phase of the flicker (see the example profiles in the top panels). As the flicker fades, the asymmetry also diminishes, typically vanishing within a few days.

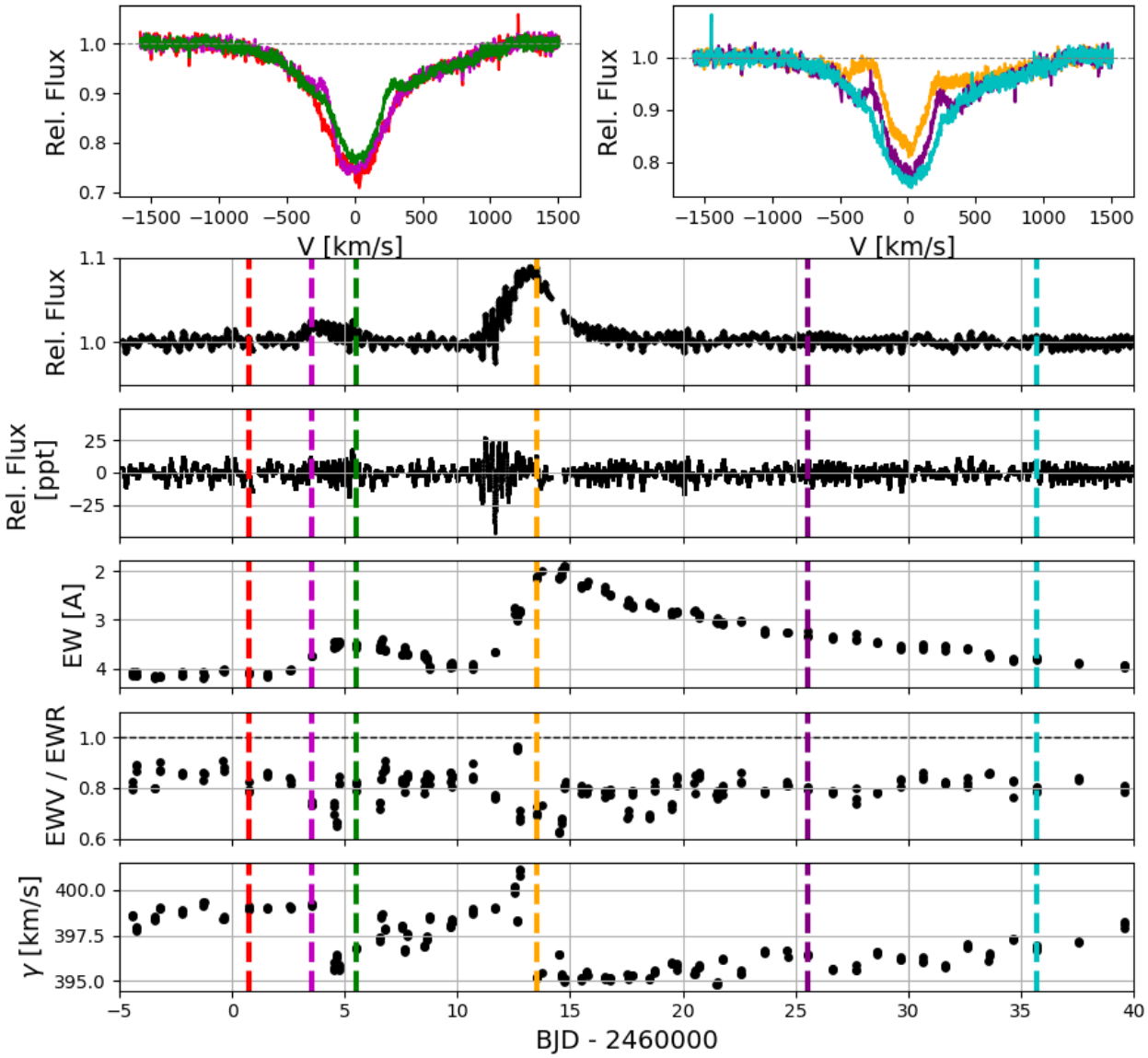


Figure 1. Observables of the Be star f Car (HD 75311). The top panels display six individual Hα spectra (three per panel). Different colors represent different observation dates marked by dashed vertical lines in the bottom panels (see [53]). The second row shows the TESS light curve with data from two consecutive sectors. The same data are shown in the third row with the long-term trends removed. The forth row illustrates the EW Hα evolution over time and the fifth presents the temporal variation of the line asymmetry (EW_V/EW_R; see Equation (1)). The last row shows the temporal variation of the metric defined in Equation (2).

Another commonly used metric in Be star research is the peak separation (PS) between the violet and red peaks of the emission line. The PS is often used as a proxy for the projected orbital velocity of the ejected material; however, it becomes ambiguous in profiles lacking a clear double peak, as first demonstrated by [54] and later quantified by [55]. In cases of single-peaked emission or when circumstellar and photospheric contributions are

of comparable strength, the PS cannot be reliably defined, resulting in the irreversible loss of critical information about the dynamics of the initial ejecta. For this reason, we adopt the following metric, inspired by Equation (1) and based on the first momentum of the line profile:

$$\gamma = \frac{\int_{v_0}^{w} v \frac{Fv}{Fc} dv}{\int_{v_0}^{w} \frac{Fv}{Fc} dv} - \frac{\int_{-w}^{v_0} v \frac{Fv}{Fc} dv}{\int_{-w}^{v_0} \frac{Fv}{Fc} dv} \quad (2)$$

where γ can be interpreted as the separation between the photocenter of each side of the line. The bottom row of Figure 1 shows the results, in which the integrals were computed with $w = 380\,\mathrm{km\,s^{-1}}$ (approximately $V_{\mathrm{orb}} \sin i$ for this star), where V_{orb} is the orbital speed at the stellar equator and i is the inclination angle. A notable property of this quantity is its sensitivity to flux increases at higher velocities. This is illustrated by the orange profile in the top-right panel, corresponding to the observation at BJD $- 2.45 \times 10^6 \sim 14$ d. This profile exhibits flux enhancements at velocities significantly greater than $V_{\mathrm{orb}} \sin i$, which is uncommon, whereas enhancements at lower velocities are universally observed during the rising phase of a flicker. This may indicate material being ejected at super-Keplerian speeds. Other examples of structures at super orbital speeds can be found in the literature, e.g., [39,56].

As a whole, the observed sample of flickers shares a common set of properties, as follows: all mass-loss events exhibited line profile asymmetries, with frequencies ranging from 0.3 to 1.9 c/d; stars displaying multiple flickers consistently showed similar EW_V/EW_R periods; all mass ejections were initially highly asymmetric, indicating localized emission regions near the stellar equator; following the peak of the flicker, the line asymmetries diminished over timescales of several days, suggesting that the ejecta gradually circularized, i.e., became more azimuthally symmetric. Furthermore, in every observed flicker, an increase in pulsation power (high-frequency signals, as clearly seen between BJD $- 2.45 \times 10^6 \sim 11$ and 13 d in the third row of Figure 1) coincided with the mass loss event—consistent with the connection between pulsation power and flickers reported in the literature (e.g., [12]).

One interesting result of [53] stemmed from a comparison between the observed line profile asymmetry periods—measured individually for all stars and flickers, and linked to the Doppler shifts of the emission lines during the ejecta's first few orbital cycles before circularization—and certain characteristic frequencies of the system, namely, the Keplerian orbital frequency at the stellar equator, the Keplerian orbital frequency at the critical radius[2], and the stellar rotational frequency. The conclusion reached was that the observed EW_V/EW_R frequency is more compatible with the Keplerian orbital frequency at the stellar equator, as illustrated in Figure 2. This in turn suggests that the material is launched by mechanisms operating very close to the stellar surface, and retains at least its characteristic orbital frequency for a few orbital cycles while remaining near the star. Although this may seem intuitive, it provides a direct observational constraint on the mass loss mechanism. In addition, it may reinforce the key role played by pulsations, which also originate in the near-surface layers of the star.

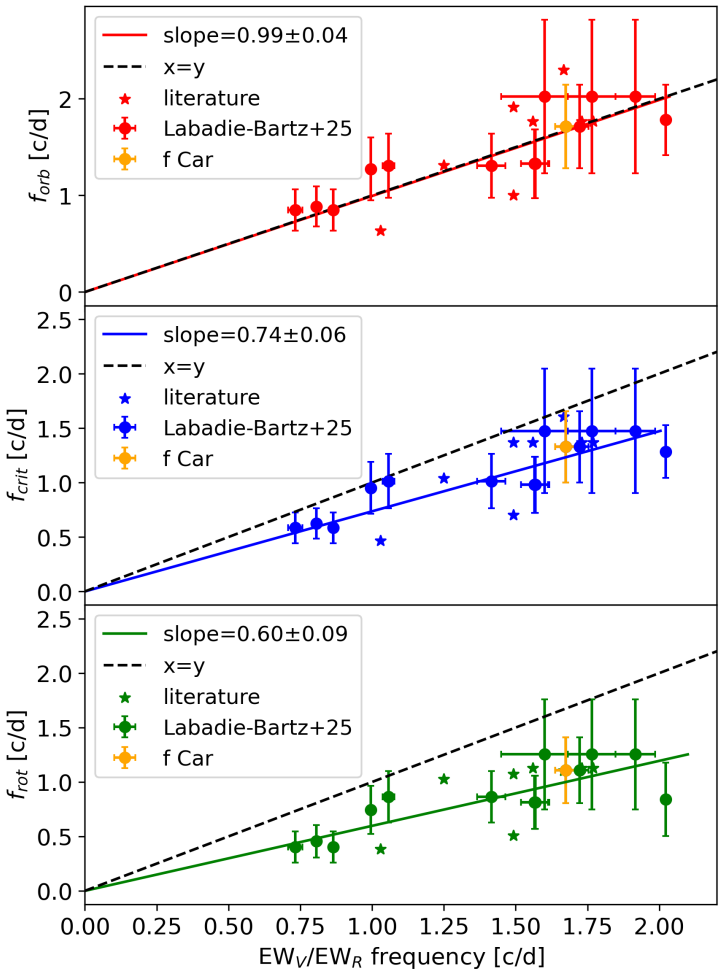


Figure 2. Three characteristic stellar frequencies (see text) compared to observed EW_V / EW_R frequencies. The solid lines are a fit to the points, while the dashed lines are the identity line. The relation approaches one-to-one for the Keplerian orbital frequency at the stellar equator (top panel). The data point corresponding to f Car is shown as orange symbols. Figure adapted from [53], ©ESO, distributed under the terms of the Creative Commons Attribution License (CC BY 4.0).

In recent months, the observational campaign has been expanded to include polarimetric monitoring. The most notable case so far is the Be star 12 Vul, shown in Figure 3. The left and top panels display variations in Hα consistent with those reported by [53]. These changes are accompanied by significant changes in both the polarization level and angle (right panels). The four bottom panels highlight the short-term variability of the observables, focusing on the periods with the largest observed changes in line emission (right) and polarization (left). Note in particular the large polarization variability—both in level and angle—seen in timescales of hours. This is reminiscent of the variations reported by [58] on Achernar. Together, these findings provide strong evidence that 12 Vul is undergoing active mass loss, in agreement with the spectroscopic indicators, and that this mass loss presents a complex geometry.

Recent Modeling Advancements

In a soon-to-be-submitted paper, Rubio et al. (in prep.) present the first direct comparison between 3D smoothed particle hydrodynamics (SPH) simulations of localized mass ejections in Be stars and observational data from the above campaign. f Car was specifically used as a template, given the quality of the observations and its clear and well-resolved flickers. Motivated by evidence that mass ejection events in Be stars are

inherently asymmetric, the simulations explore mass loss from a confined region—referred to as the injection volume—located at the stellar equator. Different values for the size and rotation rate of this injection volume as well as for the viscosity of the ejected material were explored in the simulations. The rotation rate of the injection volume may differ from that of the star itself, as it is assumed that an additional unspecified mechanism helps to lift the material into orbit.

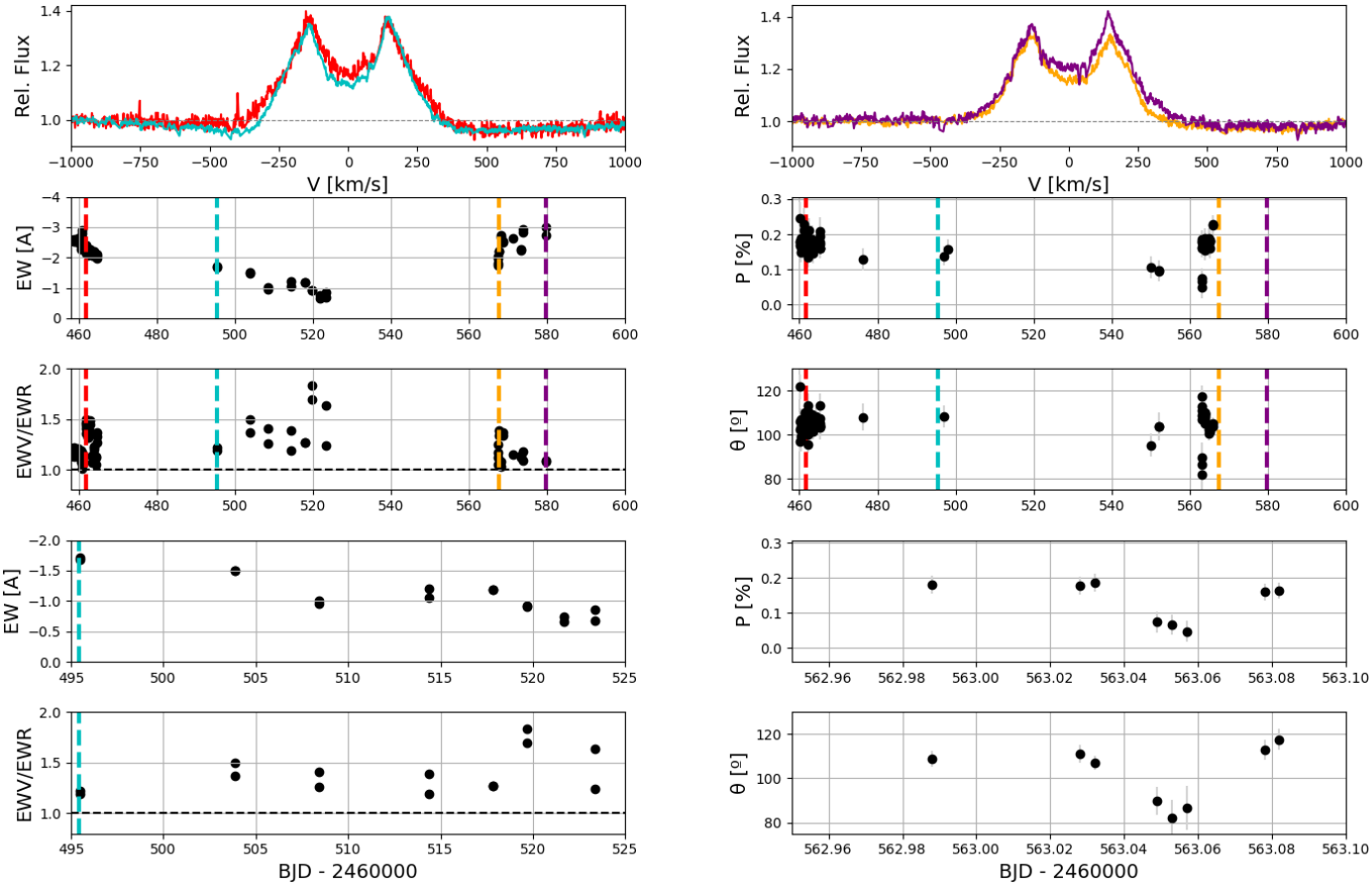


Figure 3. Observables of the Be star 12 Vul (HD 187811). The top two panels display four individual Hα spectra (two per panel). Different colors represent different observation dates marked by dashed vertical lines in the bottom panels. (**Left**): the second and third rows show the evolution of the Hα EW and asymmetry, respectively. The fourth and fifth rows focus on epochs with the largest line emission variability. (**Right**): the second and third rows display the V-band polarization level and angle, respectively. The fourth and fifth rows focus on epochs with the largest polarimetric variability.

Figure 4 shows the temporal evolution of the density of the circumstellar material in the SPH simulation that provided the closest match to the observations. In this simulation, the injection volume covers a region of 0.2 radians slightly above the stellar equator; particles are injected with a rotational velocity 5% above the angular orbital speed at the stellar equator, plus a ballistic velocity of 20 km s^{-1} with a random orientation. Using the 3D radiative transfer code HDUST [59,60], ref. [61] calculated the synthetic observables for this SPH simulation, also shown in the figure. The key observables, including the photometric light curve and Hα line profiles, equivalent widths, and asymmetries, are well-reproduced qualitatively by the model in terms of both amplitude and temporal behavior. The results suggest that localized mass injection from a restricted zone along the equator possessing mildly super-Keplerian rotation forms an important ingredient for reproducing the observed features of outbursting Be stars. It follows that early disk evolution deviates significantly from the assumptions of the steady-state viscous decretion

disk theory commonly used in the literature (e.g., [62]). This work lays a quantitative foundation for constraining the mass ejection dynamics underlying the Be phenomenon.

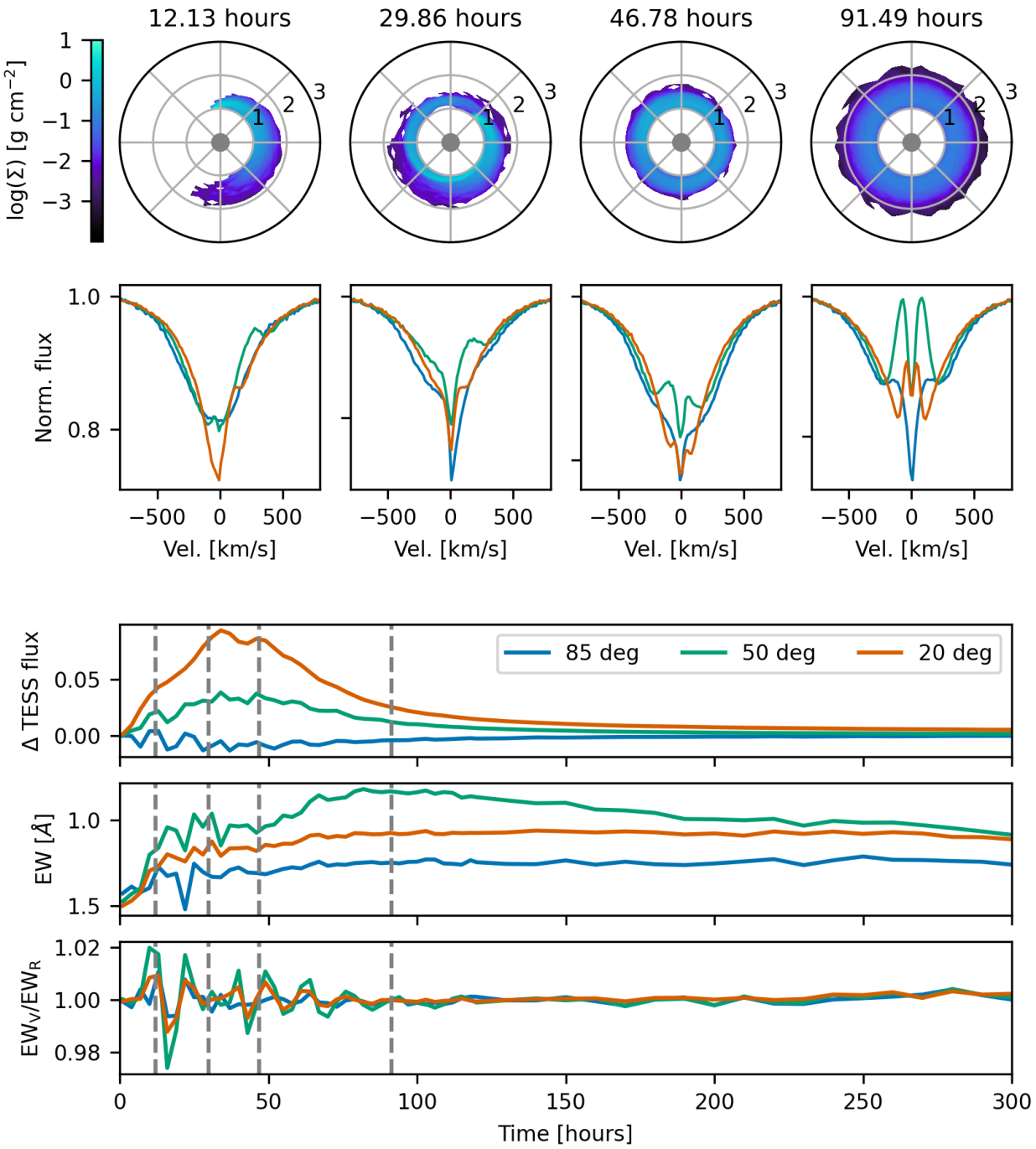


Figure 4. SPH and HDUST models of a localized mass ejection in a Be star. First row: snapshots of the temporal evolution of the surface density Σ in one of the SPH simulations of [61]. Mass is ejected from an injection volume that rotates 5% faster than the angular orbital velocity in the equator of the star. Individual particles have an added ballistic velocity of 20 km s^{-1} with a random orientation. The injection volume covers an azimuthal range of 0.2 radians around the stellar equator. Second row: Hα line profiles for each snapshot, with the line color indicating the observer inclination angle (see legend in the third row). Third to fifth rows: the temporal evolution of the photometry, Hα EW, and EW$_V$/EW$_R$ (Equation (1)), respectively. The times of each snapshots shown in the first and second rows are marked by dashed gray lines.

3. Disk Front

The previous section explored why mass loss in Be stars is now understood to occur from a relatively small region across the stellar equator, and how this manifests in observable signatures. However, what happens to the material after it is ejected—its ultimate fate—remained an open question until recently. Part of the reason for this is an intriguing consequence of the viscous decretion disk (VDD) model, as all memory of the geometry of the initial outburst is effectively erased after the ejected material circularizes and the disk begins to form. This loss of temporal information poses significant challenges to efforts aimed at reconstructing the disk formation process from the current disk structure alone, as the observable configuration no longer retains a direct imprint of the launching mechanism.

This section reviews recent high-resolution SPH simulations by [63]. SPH has been used in numerous recent studies of Be star disks [43,64–69], as it has been found to be the most adequate method to unravel the complex decretion mechanics at play when a binary companion is present. The simulations by [63] introduce three key advancements over previous work: a physically consistent treatment of the secondary star's gravitational boundary (i.e., replacing the traditional Roche lobe-sized sink with a sink matching the actual stellar radius), the inclusion of particle splitting to enhance resolution in low-density outer regions, and a revised implementation of viscosity that properly accounts for the gravitational influence of both stars. As a result, the simulations achieve unprecedented spatial coverage and dynamic resolution, probing regions up to four times farther than was previously possible.

A key outcome of these simulations is the identification and characterization of five structurally and dynamically distinct regions within the perturbed Be disk system. These regions are illustrated schematically in Figure 5 (left) and can be directly mapped onto the density distribution from one of the simulations presented in the aforementioned paper (right).

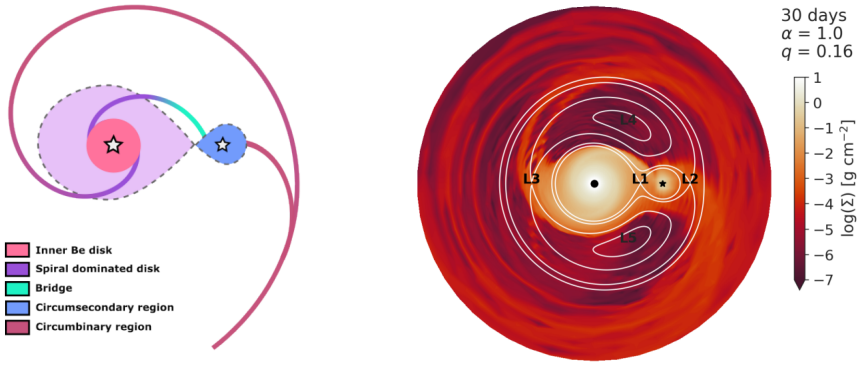


Figure 5. On the (**left**), a schematic representation of the disk, with the Be star centered and the stripped secondary on the right. On the (**right**), density maps for a model showing the Roche equipotential contours and the Lagrangian points. The Be star is the centered black dot, the secondary is the black star on the right. Figure adapted from [63], ©ESO, distributed under the terms of the Creative Commons Attribution License (CC BY 4.0).

1. Inner Be disk—This is the region closest to the Be star, and is the least perturbed by the presence of the secondary. It behaves much like the classical VDD, with near-axisymmetry and quasi-Keplerian rotation [70]. Nevertheless, the tidal torque from the companion induces the so-called accumulation effect, where material piles up in the inner disk due to the inhibition of outward angular momentum transport. This leads to a shallower surface density profile. Observationally, this results in enhanced V-band flux, different He and Fe emission line strengths, and increased polarization levels.

2. Spiral-dominated disk—Beyond a few stellar radii, the companion's gravitational potential excites large-scale two-armed spiral density waves. These structures are dynamically active, produce significant radial velocity fluctuations, and break axisymmetry. The spiral arms arise from orbital perturbations; they are tightly wound in high-viscosity disks and more open in low-viscosity systems [67]. This region can cause cyclic V/R variations in the Balmer lines and changes in the line profiles. A prime example is the locked V/R variations found in π Aqr [71] and several other Be stars [72].
3. Bridge—As one of the spiral arms extends into the Roche lobe of the secondary, a stream of material is channeled directly towards the companion. This narrow elongated structure—dubbed the bridge—acts as a conduit for angular momentum and mass exchange between the Be disk and the secondary's immediate environment. Its presence may lead to transient emission components or asymmetries in spectral lines.
4. Circumsecondary region—Material entering the companion's Roche lobe is not instantly removed, as in previous simulations ; instead, it accumulates and circularizes into a rotationally supported structure, effectively forming a small circumsecondary disk. The presence of this region is critical for understanding low-level accretion phenomena, including the possibility of faint X-ray signatures, and may offer indirect observational clues about hidden companions. Emission from this structure has been already detected in a handful of objects, such as HD 55606 [73], as well as by spectro-interferometry for HR 2142 [74].
5. Circumbinary region—Not all of the material entering the Roche lobe is accreted; a significant portion exits the lobe behind the companion, joining the trailing spiral arm and forming a large-scale one-armed spiral that wraps around the entire binary system. This circumbinary spiral is dynamically decoupled from the inner disk and constitutes the only part of the ejected matter that ultimately escapes the gravitational influence of the system. It may manifest as infrared or radio excess (see, e.g., [75]).

Taken together, these simulations outline the complete cycle of disk material in Be binaries: mass lost by the rapidly rotating Be star feeds the inner disk; part of it is deflected and captured by the companion—its former mass donor—and another fraction escapes the system in a spiral outflow.

4. Conclusions

This work presents coordinated observational and numerical advances that shed new light on two critical aspects of the Be phenomenon: the process of mass ejection from the star, and the subsequent evolution of the circumstellar disk.

Regarding the mass-loss front, the combination of space-based photometry and high-cadence spectroscopy confirms that non-radial pulsations amplified by near-critical rotation are the primary drivers of discrete mass-loss events. These episodes leave both spectroscopic and photometric signatures consistent with localized ejections near the stellar equator. Recent still-unpublished models combining SPH simulations of localized mass ejection with 3D radiative transfer calculations are well able to reproduce the observations of f Car, the star with the best-sampled mass ejection events. These models suggest that mass is ejected from the Be star at slightly super-Keplerian velocities over a small region of the equator. This localized asymmetric ejection is essential to explaining the observed line profile asymmetries.

On the disk front, state-of-the-art SPH simulations now offer sufficient resolution to resolve the full structure of Be disks in binary systems. These simulations identify five morphologically and dynamically distinct regions and demonstrate that a fraction of the ejected material is re-accreted by the secondary—the former mass donor—while

another portion escapes the system in a one-armed spiral. These results provide the first complete picture of the physical processes that connect the star and the long-term evolution of its disk.

Author Contributions: Conceptualization, A.C.C.; writing, all authors; software, A.C.R. and P.R.Q.; observations, J.L.-B. and P.R.Q.; data curation, A.C.F.S., J.L.-B. and P.R.Q. All authors have read and agreed to the published version of the manuscript.

Funding: This research was funded by 'Fundação de Amparo à Pesquisa do Estado de São Paulo', grant numbers 2021/01891-2, 2018/04055-8, 2019/13354-1, 2017/23731-1, and 2024/17860-7; 'Conselho Nacional de Pesquisa', grant number 314545/2023-9; and the 'Coordenação de Aperfeiçoamento de Pessoal de Nível Superior', grant numbers 88887.820796/2023-00, 88887.834998/2023-00, and 88887.994228/2024-00. This research was also co-funded by the European Union (ERC, MAGNIFY, Project 101126182). The views and opinions expressed are those of the authors only, and do not necessarily reflect those of the European Union or the European Research Council. Neither the European Union nor the granting authority can be held responsible for them.

Data Availability Statement: The original polarimetric data presented in this study are openly available in Vizier.

Acknowledgments: This work made use of the computing facilities of the 'Centro de processamento de Dados do IAG/USP' (CPD-IAG), the purchase of which was made possible by the Brazilian agency FAPESP (grants 2019/25950-8, 2017/24954-4, and 2009/54006-4).

Conflicts of Interest: The authors declare no conflicts of interest.

Notes

[1] V/R stands for the ratio between the blue- and red-shifted peaks in a two-peaked line profile.
[2] In the Roche approximation [57], the critical radius is defined as the maximum equatorial radius of a stable fast-spinning star, and is 50% larger than the polar radius.

References

1. Strafella, F.; Pezzuto, S.; Corciulo, G.G.; Bianchini, A.; Vittone, A.A. Stellar Winds in Herbig Ae/Be Stars. *Astrophys. J.* **1998**, *505*, 299–314. [CrossRef]
2. Kudritzki, R.P.; Puls, J. Winds from Hot Stars. *Annu. Rev. Astron. Astrophys.* **2000**, *38*, 613–666. [CrossRef]
3. Castor, J.I.; Abbott, D.C.; Klein, R.I. Radiation-driven winds in Of stars. *Astrophys. J.* **1975**, *195*, 157–174. [CrossRef]
4. Pauldrach, A.; Puls, J.; Kudritzki, R.P. Radiation-driven winds of hot luminous stars. Improvements of the theory and first results. *Astron. Astrophys.* **1986**, *164*, 86–100.
5. Vink, J.; Bocchino, F.; Damiani, F.; Kaastra, J.S. An unresolved X-ray source inside the supernova remnant RCW 86. *Astron. Astrophys.* **2000**, *362*, 711–714.
6. Vink, J.S.; de Koter, A.; Lamers, H.J.G.L.M. Mass-loss predictions for O and B stars as a function of metallicity. *Astron. Astrophys.* **2001**, *369*, 574–588. [CrossRef]
7. van Loon, J.T.; Cioni, M.R.L.; Zijlstra, A.A.; Loup, C. An empirical formula for the mass-loss rates of dust-enshrouded red supergiants and oxygen-rich Asymptotic Giant Branch stars. *Astron. Astrophys.* **2005**, *438*, 273–289. [CrossRef]
8. Humphreys, R.M.; Davidson, K. The Luminous Blue Variables: Astrophysical Geysers. *Publ. Astron. Soc. Pac.* **1994**, *106*, 1025. [CrossRef]
9. Nugis, T.; Lamers, H.J.G.L.M. Mass-loss rates of Wolf-Rayet stars as a function of stellar parameters. *Astron. Astrophys.* **2000**, *360*, 227–244.
10. Rivinius, T.; Carciofi, A.C.; Martayan, C. Classical Be stars. Rapidly rotating B stars with viscous Keplerian decretion disks. *aapr* **2013**, *21*, 69. [CrossRef]
11. Zorec, J.; Frémat, Y.; Domiciano de Souza, A.; Royer, F.; Cidale, L.; Hubert, A.M.; Semaan, T.; Martayan, C.; Cochetti, Y.R.; Arias, M.L.; et al. Critical study of the distribution of rotational velocities of Be stars. I. Deconvolution methods, effects due to gravity darkening, macroturbulence, and binarity. *Astron. Astrophys.* **2016**, *595*, A132. [CrossRef]
12. Labadie-Bartz, J.; Carciofi, A.C.; Henrique de Amorim, T.; Rubio, A.; Luiz Figueiredo, A.; Ticiani dos Santos, P.; Thomson-Paressant, K. Classifying Be Star Variability with TESS. I. The Southern Ecliptic. *Astron. J.* **2022**, *163*, 226. [CrossRef]

13. Bodenheimer, P. Rapidly Rotating Stars. VII. Effects of Angular Momentum on Upper-Main Models. *Astrophys. J.* **1971**, *167*, 153. [CrossRef]
14. Pols, O.R.; Cote, J.; Waters, L.B.F.M.; Heise, J. The formation of Be stars through close binary evolution. *Astron. Astrophys.* **1991**, *241*, 419–438.
15. Ekström, S.; Meynet, G.; Maeder, A.; Barblan, F. Evolution towards the critical limit and the origin of Be stars. *Astron. Astrophys.* **2008**, *478*, 467–485. [CrossRef]
16. Sana, H.; de Mink, S.E.; de Koter, A.; Langer, N.; Evans, C.J.; Gieles, M.; Gosset, E.; Izzard, R.G.; Le Bouquin, J.B.; Schneider, F.R.N. Binary Interaction Dominates the Evolution of Massive Stars. *Science* **2012**, *337*, 444. [CrossRef]
17. Hastings, B.; Langer, N.; Wang, C.; Schootemeijer, A.; Milone, A.P. Stringent upper limit on Be star fractions produced by binary interaction. *Astron. Astrophys.* **2021**, *653*, A144. [CrossRef]
18. Bodensteiner, J.; Shenar, T.; Sana, H. Investigating the lack of main-sequence companions to massive Be stars. *Astron. Astrophys.* **2020**, *641*, A42. [CrossRef]
19. Dodd, J.M.; Oudmaijer, R.D.; Radley, I.C.; Vioque, M.; Frost, A.J. Gaia uncovers difference in B and Be star binarity at small scales: evidence for mass transfer causing the Be phenomenon. *Mon. Not. R. Astron. Soc.* **2024**, *527*, 3076–3086. [CrossRef]
20. Preece, H.P.; Hamers, A.S.; Battich, T.; Rajamuthukumar, A.S. Forming hot subluminous stars from hierarchical triples—I. The role of an outer tertiary on formation channels. *Mon. Not. R. Astron. Soc.* **2022**, *517*, 2111–2120. [CrossRef]
21. Granada, A.; Ekström, S.; Georgy, C.; Krtička, J.; Owocki, S.; Meynet, G.; Maeder, A. Populations of rotating stars. II. Rapid rotators and their link to Be-type stars. *Astron. Astrophys.* **2013**, *553*, A25. [CrossRef]
22. Hastings, B.; Wang, C.; Langer, N. The single star path to Be stars. *Astron. Astrophys.* **2020**, *633*, A165. [CrossRef]
23. Zhao, X.; Fuller, J. Centrifugally driven mass-loss and outbursts of massive stars. *Mon. Not. R. Astron. Soc.* **2020**, *495*, 249–265. [CrossRef]
24. Georgy, C.; Ekström, S.; Granada, A.; Meynet, G.; Mowlavi, N.; Eggenberger, P.; Maeder, A. Populations of rotating stars. I. Models from 1.7 to 15 Msun at Z = 0.014, 0.006, and 0.002 with Ω/Ω_{crit} between 0 and 1. *Astron. Astrophys.* **2013**, *553*, A24. [CrossRef]
25. Rímulo, L.R.; Carciofi, A.C.; Vieira, R.G.; Rivinius, T.; Faes, D.M.; Figueiredo, A.L.; Bjorkman, J.E.; Georgy, C.; Ghoreyshi, M.R.; Soszyński, I. The life cycles of Be viscous decretion discs: Fundamental disc parameters of 54 SMC Be stars. *Mon. Not. R. Astron. Soc.* **2018**, *476*, 3555–3579. [CrossRef]
26. Corsaro, E.; Mathur, S.; García, R.A.; Gaulme, P.; Pinsonneault, M.; Stassun, K.; Stello, D.; Tayar, J.; Trampedach, R.; Jiang, C.; et al. Metallicity effect on stellar granulation detected from oscillating red giants in open clusters. *Astron. Astrophys.* **2017**, *605*, A3. [CrossRef]
27. Bjorkman, J.E.; Cassinelli, J.P. Equatorial Disk Formation around Rotating Stars Due to Ram Pressure Confinement by the Stellar Wind. *Astrophys. J.* **1993**, *409*, 429. [CrossRef]
28. Owocki, S.P.; Cranmer, S.R.; Gayley, K.G. Inhibition FO Wind Compressed Disk Formation by Nonradial Line-Forces in Rotating Hot-Star Winds. *Astrophys. J. Lett.* **1996**, *472*, L115. [CrossRef]
29. Cranmer, S.R.; Owocki, S.P. The Effect of Oblateness and Gravity Darkening on the Radiation Driving in Winds from Rapidly Rotating B Stars. *Astrophys. J.* **1995**, *440*, 308. [CrossRef]
30. Grady, C.A.; Bjorkman, K.S.; Snow, T.P. Highly Ionized Stellar Winds in Be Stars: The Evidence for Aspect Dependence. *Astrophys. J.* **1987**, *320*, 376. [CrossRef]
31. Kee, N.D.; Owocki, S.; Sundqvist, J.O. Line-driven ablation of circumstellar discs—I. Optically thin decretion discs of classical Oe/Be stars. *Mon. Not. R. Astron. Soc.* **2016**, *458*, 2323–2335. [CrossRef] [PubMed]
32. Kee, N.D.; Owocki, S.; Kuiper, R. Line-driven ablation of circumstellar discs—II. Analysing the role of multiple resonances. *Mon. Not. R. Astron. Soc.* **2018**, *474*, 847–853. [CrossRef]
33. Martayan, C.; Frémat, Y.; Hubert, A.M.; Floquet, M.; Zorec, J.; Neiner, C. Effects of metallicity, star-formation conditions, and evolution in B and Be stars. II. Small Magellanic Cloud, field of NGC 330. *Astron. Astrophys.* **2007**, *462*, 683–694. [CrossRef]
34. Cassinelli, J.P.; Brown, J.C.; Maheswaran, M.; Miller, N.A.; Telfer, D.C. A Magnetically Torqued Disk Model for Be Stars. *Astrophys. J.* **2002**, *578*, 951–966. [CrossRef]
35. Rogers, T.M.; Lin, D.N.C.; McElwaine, J.N.; Lau, H.H.B. Internal Gravity Waves in Massive Stars: Angular Momentum Transport. *Astrophys. J.* **2013**, *772*, 21. [CrossRef]
36. Owocki, S. Formation and Evolution of Disks around Classical Be Stars. *Astron. Soc. Pac. Conf. Ser.* **2006**, *355*, 219.
37. Baade, D. Does 28 CMa have a photometric period differing from its spectroscopic period ? *Astron. Astrophys.* **1982**, *110*, L15–L17.
38. Rivinius, T.; Baade, D.; Štefl, S. Non-radially pulsating Be stars. *Astron. Astrophys.* **2003**, *411*, 229–247. [CrossRef]
39. Rivinius, T.; Baade, D.; Stefl, S.; Stahl, O.; Wolf, B.; Kaufer, A. Stellar and circumstellar activity of the Be star MU Centauri. I. Line emission outbursts. *Astron. Astrophys.* **1998**, *333*, 125–140.

40. Baade, D.; Rivinius, T.; Pigulski, A.; Carciofi, A.C.; Martayan, C.; Moffat, A.F.J.; Wade, G.A.; Weiss, W.W.; Grunhut, J.; Handler, G.; et al. Short-term variability and mass loss in Be stars. I. BRITE satellite photometry of η and μ Centauri. *Astron. Astrophys.* **2016**, *588*, A56. [CrossRef]
41. Lee, U.; Osaki, Y.; Saio, H. Viscous excretion discs around Be stars. *Mon. Not. R. Astron. Soc.* **1991**, *250*, 432–437. [CrossRef]
42. Haubois, X.; Carciofi, A.C.; Rivinius, T.; Okazaki, A.T.; Bjorkman, J.E. Dynamical Evolution of Viscous Disks around Be Stars. I. Photometry. *Astrophys. J.* **2012**, *756*, 156. [CrossRef]
43. Okazaki, A.T.; Bate, M.R.; Ogilvie, G.I.; Pringle, J.E. Viscous effects on the interaction between the coplanar decretion disc and the neutron star in Be/X-ray binaries. *Mon. Not. R. Astron. Soc.* **2002**, *337*, 967–980. [CrossRef]
44. Carciofi, A.C.; Bjorkman, J.E.; Otero, S.A.; Okazaki, A.T.; Štefl, S.; Rivinius, T.; Baade, D.; Haubois, X. The First Determination of the Viscosity Parameter in the Circumstellar Disk of a Be Star. *Astrophys. J. Lett.* **2012**, *744*, L15. [CrossRef]
45. Haubois, X.; Mota, B.C.; Carciofi, A.C.; Draper, Z.H.; Wisniewski, J.P.; Bednarski, D.; Rivinius, T. Dynamical Evolution of Viscous Disks around Be Stars. II. Polarimetry. *Astrophys. J.* **2014**, *785*, 12. [CrossRef]
46. Marr, K.C.; Jones, C.E.; Carciofi, A.C.; Rubio, A.C.; Mota, B.C.; Ghoreyshi, M.R.; Hatfield, D.W.; Rímulo, L.R. The Be Star 66 Ophiuchi: 60 Years of Disk Evolution. *Astrophys. J.* **2021**, *912*, 76. [CrossRef]
47. Rubio, A.C.; Carciofi, A.C.; Ticiani, P.; Mota, B.C.; Vieira, R.G.; Faes, D.M.; Genaro, M.; de Amorim, T.H.; Klement, R.; Araya, I.; et al. Bayesian sampling with BeAtlas, a grid of synthetic Be star spectra I. Recovering the fundamental parameters of α Eri and β CMi. *Mon. Not. R. Astron. Soc.* **2023**, *526*, 3007–3036. [CrossRef]
48. Figueiredo, A.L.; Carciofi, A.C.; Labadie-Bartz, J.; Pinho, M.L.; de Amorin, T.H.; dos Santos, P.T.; Soszyński, I.; Udalski, A. Be star demographics: A comprehensive study of thousands of lightcurves in the Magellanic Clouds. *arXiv* **2025**, arXiv:2505.08714. [CrossRef]
49. Ricker, G.R.; Winn, J.N.; Vanderspek, R.; Latham, D.W.; Bakos, G.Á.; Bean, J.L.; Berta-Thompson, Z.K.; Brown, T.M.; Buchhave, L.; Butler, N.R.; et al. Transiting Exoplanet Survey Satellite (TESS). *J. Astron. Telesc. Instruments Syst.* **2015**, *1*, 014003. [CrossRef]
50. Siverd, R.J.; Brown, T.M.; Barnes, S.; Bowman, M.K.; De Vera, J.; Foale, S.; Harbeck, D.R.; Henderson, T.; Hygelund, J.; Kirby, A.; et al. NRES: The network of robotic echelle spectrographs. In Proceedings of the SPIE Astronomical Telescopes + Instrumentation, Austin, TX, USA, 10–15 June 2018; Volume 10702, p. 107026C. [CrossRef]
51. Vieira, R.G.; Carciofi, A.C.; Bjorkman, J.E. The pseudo-photosphere model for the continuum emission of gaseous discs. *Mon. Not. R. Astron. Soc.* **2015**, *454*, 2107–2119. [CrossRef]
52. Zamanov, R.K.; Stoyanov, K.A.; Stefanov, S.Y.; Bode, M.F.; Minev, M.S. Optical spectroscopy of Be stars: Peak separation of Balmer emission lines. *Astron. Nachr.* **2023**, *344*. [CrossRef]
53. Labadie-Bartz, J.; Carciofi, A.C.; Rubio, A.C.; Baade, D.; Siverd, R.; Arcos, C.; Figueiredo, A.L.; Nazé, Y.; Neiner, C.; Rivinius, T.; et al. The birth of Be star disks I. From localized ejection to circularization. *arXiv* **2025**, arXiv:2504.07571. [CrossRef]
54. Slettebak, A. BE Stars as Rotating Stars: Observations (review Paper). *Symp. Int. Astron. Union* **1976**, *70*, 123–136. [CrossRef]
55. Hanuschik, R.W.; Kozok, J.R.; Kaiser, D. High-resolution emission-line spectroscopy of Be stars. III—Balmer line profiles. *Astron. Astrophys.* **1988**, *189*, 147–162.
56. Štefl, S.; Baade, D.; Rivinius, T.; Otero, S.; Stahl, O.; Budovičová, A.; Kaufer, A.; Maintz, M. Stellar and circumstellar activity of the Be star omega CMa. I. Line and continuum emission in 1996–2002. *Astron. Astrophys.* **2003**, *402*, 253–265. [CrossRef]
57. Roche, E. Recherches sur les atmospheres des cometes. *Ann. L'Obs. Paris* **1859**, *5*, 353–393.
58. Carciofi, A.C.; Magalhães, A.M.; Leister, N.V.; Bjorkman, J.E.; Levenhagen, R.S. Achernar: Rapid Polarization Variability as Evidence of Photospheric and Circumstellar Activity. *Astrophys. J. Lett.* **2007**, *671*, L49–L52. [CrossRef]
59. Carciofi, A.C.; Bjorkman, J.E. Non-LTE Monte Carlo Radiative Transfer. I. The Thermal Properties of Keplerian Disks around Classical Be Stars. *Astrophys. J.* **2006**, *639*, 1081–1094. [CrossRef]
60. Carciofi, A.C.; Bjorkman, J.E. Non-LTE Monte Carlo Radiative Transfer. II. Nonisothermal Solutions for Viscous Keplerian Disks. *Astrophys. J.* **2008**, *684*, 1374–1383. [CrossRef]
61. Rubio, A.C.; Carciofi, A.C.; Baade, D.; Labadie-Bartz, J.; de Amorim, T.H. The birth of Be star disks — II. SPH models of localized mass ejections. *in preparation* **2025**.
62. Carciofi, A.C. The circumstellar discs of Be stars. *Proc. Int. Astron. Union* **2010**, *6*, 325–336. [CrossRef]
63. Rubio, A.C.; Carciofi, A.C.; Bjorkman, J.E.; de Amorim, T.H.; Okazaki, A.T.; Suffak, M.W.; Jones, C.E.; Candido, P.P. High-spatial-resolution simulations of Be star disks in binary systems: I. Structure and kinematics of coplanar disks. *Astron. Astrophys.* **2025**, *698*, 309. [CrossRef]
64. Panoglou, D.; Carciofi, A.C.; Vieira, R.G.; Cyr, I.H.; Jones, C.E.; Okazaki, A.T.; Rivinius, T. Be discs in binary systems—I. Coplanar orbits. *Mon. Not. R. Astron. Soc.* **2016**, *461*, 2616–2629. [CrossRef]
65. Cyr, I.H.; Jones, C.E.; Panoglou, D.; Carciofi, A.C.; Okazaki, A.T. Be discs in binary systems—II. Misaligned orbits. *Mon. Not. R. Astron. Soc.* **2017**, *471*, 596–605. [CrossRef]
66. Panoglou, D.; Faes, D.M.; Carciofi, A.C.; Okazaki, A.T.; Baade, D.; Rivinius, T.; Borges Fernandes, M. Be discs in coplanar circular binaries: Phase-locked variations of emission lines. *Mon. Not. R. Astron. Soc.* **2018**, *473*, 3039–3050. [CrossRef]

67. Cyr, I.H.; Jones, C.E.; Carciofi, A.C.; Steckel, C.; Tycner, C.; Okazaki, A.T. Spiral density enhancements in Be binary systems. *Mon. Not. R. Astron. Soc.* **2020**, *497*, 3525–3536. [CrossRef]
68. Suffak, M.; Jones, C.E.; Carciofi, A.C. Growth and dissipation of Be star discs in misaligned binary systems. *Mon. Not. R. Astron. Soc.* **2022**, *509*, 931–944. [CrossRef]
69. Suffak, M.W.; Jones, C.E.; Carciofi, A.C. Investigating Kozai-Lidov oscillations and disc tearing in Be star discs. *Mon. Not. R. Astron. Soc.* **2025**, *536*, 2234–2259. [CrossRef]
70. Wheelwright, H.E.; Bjorkman, J.E.; Oudmaijer, R.D.; Carciofi, A.C.; Bjorkman, K.S.; Porter, J.M. Probing the properties of Be star discs with spectroastrometry and NLTE radiative transfer modelling: β CMi. *Mon. Not. R. Astron. Soc.* **2012**, *423*, L11–L15. [CrossRef]
71. Zharikov, S.V.; Miroshnichenko, A.S.; Pollmann, E.; Danford, S.; Bjorkman, K.S.; Morrison, N.D.; Favaro, A.; Guarro Fló, J.; Terry, J.N.; Desnoux, V.; et al. Doppler tomography of the circumstellar disk of π Aquarii. *Astron. Astrophys.* **2013**, *560*, A30. [CrossRef]
72. Miroshnichenko, A.S.; Chari, R.; Danford, S.; Prendergast, P.; Aarnio, A.N.; Andronov, I.L.; Chinarova, L.L.; Lytle, A.; Amantayeva, A.; Gabitova, I.A.; et al. Searching for Phase-Locked Variations of the Emission-Line Profiles in Binary Be Stars. *Galaxies* **2023**, *11*, 83. [CrossRef]
73. Chojnowski, S.D.; Labadie-Bartz, J.; Rivinius, T.; Gies, D.; Panoglou, D.; Borges Fernandes, M.; Wisniewski, J.P.; Whelan, D.G.; Mennickent, R.E.; McMillan, R.; et al. The Remarkable Be+sdOB Binary HD 55606. I. Orbital and Stellar Parameters. *Astrophys. J.* **2018**, *865*, 76. [CrossRef]
74. Klement, R.; Rivinius, T.; Gies, D.R.; Baade, D.; Mérand, A.; Monnier, J.D.; Schaefer, G.H.; Lanthermann, C.; Anugu, N.; Kraus, S.; et al. The CHARA Array Interferometric Program on the Multiplicity of Classical Be Stars: New Detections and Orbits of Stripped Subdwarf Companions. *Astrophys. J.* **2024**, *962*, 70. [CrossRef]
75. Klement, R.; Carciofi, A.C.; Rivinius, T.; Ignace, R.; Matthews, L.D.; Torstensson, K.; Gies, D.; Vieira, R.G.; Richardson, N.D.; Domiciano de Souza, A.; et al. Prevalence of SED Turndown among Classical Be Stars: Are All Be Stars Close Binaries? *Astrophys. J.* **2019**, *885*, 147. [CrossRef]

Disclaimer/Publisher's Note: The statements, opinions and data contained in all publications are solely those of the individual author(s) and contributor(s) and not of MDPI and/or the editor(s). MDPI and/or the editor(s) disclaim responsibility for any injury to people or property resulting from any ideas, methods, instructions or products referred to in the content.